INSTITUTE OF PHYSICS PUBLISHING MEASUREMENT SCIENCE AND TECHNOLOGY

Meas. Sci. Technol. **17** (2006) 1733–1740 doi:10.1088/0957-0233/17/7/011

Development of a fibre Bragg grating sensored ground movement monitoring system

Yen-Te Ho, An-Bin Huang and Jui-Ting Lee

Department of Civil Engineering, National Chiao-Tung University, Hsinchu, Taiwan, Republic of China

E-mail: yenteho@pchome.com.tw, abhuang@mail.nctu.edu.tw and ruiting.cv92g@nctu.edu.tw

Received 19 December 2005, in final form 28 March 2006
Published 7 June 2006
Online at stacks.iop.org/MST/17/1733

Abstract

Monitoring ground movement manually by lowering an inclinometer probe (IP) in a grouted-in-place casing has been in practice for decades. It is possible to install multiple IP units at various depths in an inclinometer casing to allow automated data logging. The high cost and other problems associated with transmitting signals electrically make an automated IP rather impractical for long term and/or massive deployment. In addition to its small size, available technologies allow optical signals to be transmitted over many kilometres and not be affected by electromagnetic interference. The optical fibre Bragg grating (FBG) is one of the many available fibre optic sensor technologies. The authors used FBG as a sensing medium and developed a ground movement monitoring device referred to as the FBG segmented deflectometer (FBG-SD). The FBG-SD, designed to be inserted into the conventional inclinometer casing, measures the relative deflection between the segments. The amount of lateral movement is computed on the basis of the distribution of the segmented deflections. To verify the effectiveness of the new system, the authors performed indoor as well as field experiments where results from FBG-SDs were compared with conventional IP readings. This paper introduces the design principles of the FBG-SD and describes the performance of the system in their indoor and field applications.

Keywords: fibre Bragg grating, segmented deflectometer, ground movement monitoring

Introduction

According to Green and Mickkelsen (1988), S D Wilson of Harvard University developed the concept of a probe inclinometer in 1952. Today, the inclinometer is probably the most widely used technique in the analysis and detection of ground movement. A plastic or aluminium casing is installed in a near vertical position in the ground. A servo-accelerometer sealed in a carriage referred to as the inclinometer probe (IP) is typically used to serve as the sensor unit and measures the inclination. The IP is equipped with wheels that fit tightly with the grooves in the casing. An electric cable raises and lowers the IP in the casing and transmits electric signals to the surface. The IP system monitors the casing response to the ground movement. Readings from the sensor unit are taken at a fixed interval as the probe is raised or lowered in the casing. The sensor unit measures its inclination angle, $\delta\theta$, with respect to verticality. The distance between successive readings, L, multiplied by sin $\delta\theta$, equals the relative lateral displacement in that interval. The displacement at any depth of the casing is determined by accumulating the relative displacements from a reference point (usually the bottom of the casing) to that depth. The commercially available IP can have a resolution of approximately 0.002° or capable of detecting changes in

inclination on the order of 1:25 000. The precision of IP can range from 2 to 6 mm for a 30 m measurement (Dunnicliff 1988)

In cases where it is not feasible to dispatch technicians for field measurements, or where continuous readings are required, a series of servo-accelerometers or electrolytic sensors can be placed in the casing on a long-term basis to monitor ground movement. The concept typically referred to as an in-place inclinometer (IPI), involves the use of multiple sensor units that are aligned and secured in the inclinometer casing by spring-loaded wheels. The principles involved in obtaining readings and determining lateral displacements are similar to those of the IP. The main difference is that the distance between successive readings of L is now determined by the fixed positions of the in-place sensor units instead of being controlled by the amount of raising or lowering of the electric cable. Because there is no need for manual setting of the position of the in-place sensor units when taking the readings, the system operation and data logging can be automated. Eliminating the need for sensor placement enhances the stability of the inclination readings by IPI (Mickkelsen 1996). The high cost of IPI often prohibits the system from being used to obtain a continuous profile of deformation. Rather, the intention is to measure critical movements of a few sections within the inclinometer casing.

The deflectometer is another monitoring electrical instrument that has been reported and used for the measurement of ground movement (Dutro 1977, Dunnicliff 1988, Kumbhojkar *et al* 1991). The deflectometer consists of a flexible element that connects to a rigid segment at both ends. The amount of deflection of the flexible element or relative rotation between two neighbouring rigid segments is typically sensored by strain gauges. As in the case of IP, the deflectometer can be used inside an inclinometer casing. The lateral movement of the inclinometer casing is computed on the basis of the deflection experienced by the flexible elements. An important advantage of the deflectometer is that it can be used horizontally, vertically, or at any angle of inclination. A disadvantage is that the error of measurement is accumulative when using the relative rotation as the basis for lateral movement computation.

The above-described ground movement monitoring devices use an electrical system for sensing and signal transmission. The electrical system is prone to short circuit when exposed to a humid environment such as underground or below ground water. Most of the electrical sensors are non-distributive in nature where one transmission line is dedicated to a specific sensor. When a large number of sensors are used, an equally large number of transmission lines can make the system impractical. The electrical signals are subject to electromagnetic interference. These drawbacks make the automated electrical ground movement monitoring systems difficult or costly to use.

The optical fibre to be described in this paper is made of 125 μm diameter silica covered with a coat of acrylic. The outside diameter of the optical fibre is 250 μm. The light signal is immune to electromagnetic interference and can be transmitted for tens of kilometres through an optical fibre. These characteristics make optical fibre an ideal medium for geotechnical instrumentation in the field. There have been reports on monitoring ground movement using optical fibre sensors. Most of these developments used optical fibre sensors as a qualitative indicator. The optical fibres are laid on the surface of a slope; failure of the slope surface would stretch the fibres. The slope stability is thus monitored by detecting the stretching of the optical fibres (Naruse *et al* 2000, Kihara *et al* 2002). Yoshida *et al* (2002) developed a mechanism to quantitatively monitor deflection using a pair of optical fibres as shown in figure 1, following the principle of the conventional deflectometer. This mechanism has the same function as the flexible element of a deflectometer. The amount of relative rotation, or rotation of the bottom piece around the hinge in figure 1, is determined by the differential elongation between the two pre-stressed optical fibres. Because of the flexible nature of the optical fibre, the measurement mechanism is effective only if the optical fibres remain tensioned. The weight of the sensor units and friction between the sensor support and the grooves in the inclinometer casing can all affect the tension in the optical fibres and thus their readings for the design of figure 1.

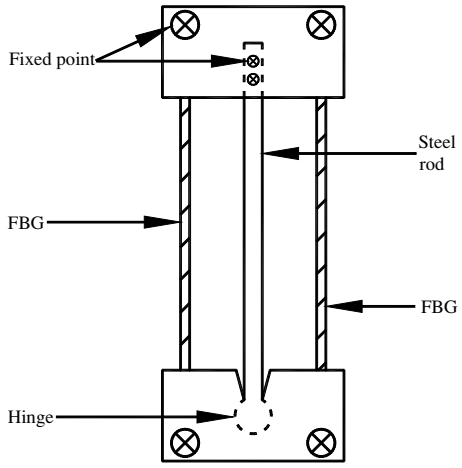

Figure 1. Deflection monitoring using a pair of FBGs (after Yoshida *et al* (2002)).

The researchers used FBG as a strain sensor and developed a segmented deflectometer, referred to as the FBG-SD. The design of the FBG-SD evolved from the conventional deflectometer, but took advantage of the additional capabilities of FBG. The main purpose of the FBG-SD is to monitor ground movement. This paper provides a brief background on the principles of FBG strain sensors, and presents details of the FBG-SD design and laboratory/field verifications of its effectiveness.

The optical fibre Bragg grating (FBG) strain sensor

Significant progress in the development of optical fibre sensors has been made in the past 20 years (Measures 2001). The fibre Bragg grating (FBG) is one of the many available optical fibre sensor techniques. Hill *et al* (1978) reported that light launched into a fibre can be reflected due to a refractive index grating written into the core of the optical fibre. Meltz *et al* (1989) pioneered the technique of producing in-fibre Bragg gratings by holographic writing, making it possible to produce FBGs useful for telecommunications. FBG lengths are normally within a range of 1–20 mm. Periodic variation

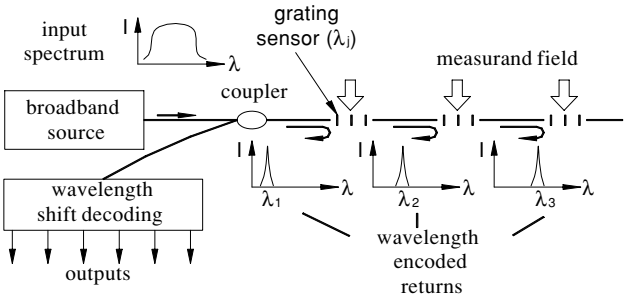

Figure 2. The conceptual description of FBG sensors (after Kersey (1992)).

or modulation of a fibre core refractive index is formed by exposing a segment of a single mode optical fibre (Rao 1998) to a spatial pattern of ultraviolet light. When the FBG is illuminated by a wideband light source, a fraction of the light is reflected back upon interference by the FBG. The wavelength of the reflected light, or the Bragg wavelength, λ_B, is related to the period of the index modulation, Λ, and effective fibre core index of refraction, n, as

$$\lambda_B = 2n\Lambda. \tag{1}$$

Longitudinal strain within the Bragg grating, ε_B, induced by variations in temperature or stress can cause a change in Λ and thus a shifting of λ_B or $\Delta\lambda_B$ in nanometres (10^{-9} m), with the following approximate relationships (Rao 1998):

$$\Delta\lambda_B = 0.74\lambda_B\varepsilon_B \quad \text{or} \quad \varepsilon_B = \frac{\Delta\lambda_B}{0.74\,\lambda_B} \tag{2}$$

and

$$\Delta\lambda_B = 8.9 \times 10^{-6}\lambda_B\,\Delta T \tag{3}$$

where ΔT is the change of temperature in degrees Celsius. The constants in equations (2) and (3) can vary, depending on the photoelastic properties of the optical fibre. For the FBGs reported herein, λ_B ranged from 1525 to 1575 nm. The returned signal from every FBG carries a unique range or domain of wavelength $\lambda_B + \Delta\lambda_B$, making it possible to have multiple FBG elements on the same fibre. The multiplexing among various sensors on a single fibre can be accomplished by wavelength division addressing as conceptually described in figure 2. Most silica optical fibres break at a strain of 0.01 which corresponds to a $\Delta\lambda_B$ of approximately 10 nm. Thus, a 2 to 3 nm separation of λ_B between FBGs would suffice in most cases. There is a limited bandwidth of the light source and as the light passes an FBG there is a loss of intensity. The number of FBG sensors that can be placed on a fibre with the available FBG interrogation systems is not more than 20.

A digitally controlled interrogator is used to provide the light source and interpret the signals reflected by the FBGs. The FBG readings from the interrogator are transmitted to a computer. The design principles of the FBG interrogators are beyond the scope of this paper. Readers are referred to Rao (1998), Othonos and Kalli (1999) and Dyer *et al* (2005) for details and recent developments in FBG interrogation. The main function of an FBG interrogator is to measure the peak wavelength or $\lambda_B + \Delta\lambda_B$ reflected by the FBGs. Ground movement monitoring is basically a long term and static measurement. For the FBG-SD, the peak wavelength interrogation should have a resolution of 1 pm (10^{-12} m) with

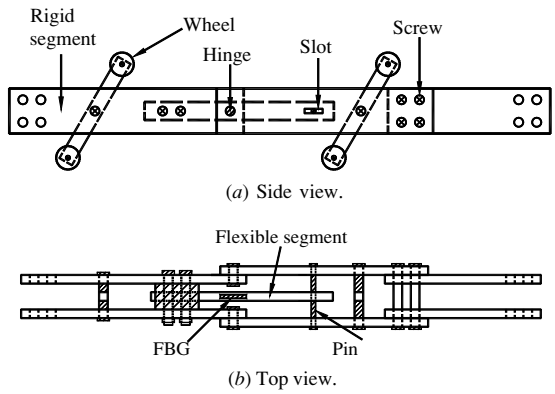

Figure 3. Schematic views of a single FBG-SD unit: (*a*) side view, (*b*) top view.

drift not exceeding 5 pm. Some of the recent, commercially available FBG interrogators are capable of meeting these requirements.

FBG has the advantages of optical fibre sensors as previously described plus the fact that there can be multiple FBG elements on the same fibre. According to equation (1) and the possible range of λ_B, approximately 0.86 μm m^{-1} can be resolved with the currently available FBG interrogating system for 1 pm of $\Delta\lambda_B$. Thus, the resolution of FBG can be at least as good as that of strain gauges. These unique features make FBG rather attractive as a means for monitoring civil engineering systems. According to equation (3), 1 °C in ΔT should correspond to approximately 14 pm in $\Delta\lambda_B$. When packaged with epoxy as in the case of the FBG-SD, an FBG becomes even more sensitive to temperature changes. The design of the FBG-SD made an attempt to minimize the temperature effects.

Design of the fibre Bragg grating segmented deflectometer (FBG-SD)

Because of the long history and popularity of inclinometer casings, the FBG-SD is designed to be used in a conventional inclinometer casing. As shown in figure 3, a single unit of the FBG-SD consists of a plastic rod (the flexible segment) that connects to two aluminium end pieces (the rigid segments). The rigid segments are equipped with wheeled braces so that the FBG-SD can be fitted to the grooves in the inclinometer casing. Two FBGs are attached to the opposite sides of a plastic rod or the flexible segment (figure 3) to measure the flexural strain. The diameter and length of the plastic rod can be changed to optimize the strain resolution of the FBG-SD. The length of the aluminium end pieces can be varied to adjust for the space resolution. One end of the plastic rod is fixed to a rigid segment where no sliding or rotation is allowed. The other end of the plastic rod is supported on the neighbouring rigid segment with a pin-in-the-slot where longitudinal sliding and rotation are allowed. The rigid segments are connected with hinges which allow rotation only in the plane that includes the two opposite grooves of the inclinometer casing or FBGs. Or, the FBG-SD is designed to monitor ground movement only in the plane where the rigid segments are allowed to rotate. The distortion of the inclinometer casing induced

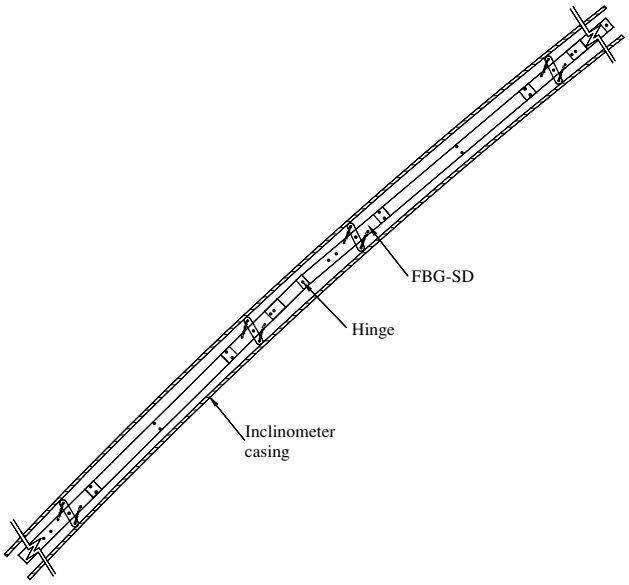

Figure 4. Interaction between the FBG-SD and inclinometer casing.

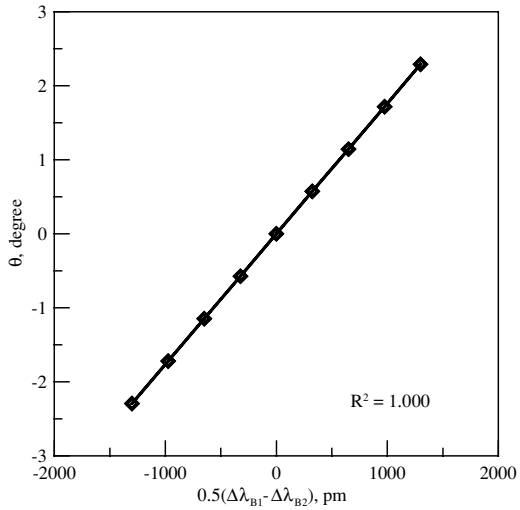

Figure 5. Calibration result of an FBG-SD unit.

by ground movement causes a relative rotation between the rigid segments of the inserted FBG-SD as shown in figure 4. This relative rotation creates bending in the flexible segment which behaves as a cantilever. The bending, in turn, causes flexural strains in the FBGs attached to the surface of the flexible segment. Because the pin-supported end of the flexible segment is free to slide longitudinally in the slot, the weight of the FBG-SD elements and friction between the brace wheels and the casing grooves would have no effect on the flexural strains.

The use of the FBG-SD involves the following process:

(1) *Calibration of the single FBG-SD*: every set of the FBG-SD (one flexible segment with two neighbouring rigid segments) is calibrated upon assembly to establish the relationship between the angle of segment rotation around the hinge and the change in wavelength as experienced by the FBGs attached to the flexible segment.

(2) *Assembly and insertion of the FBG-SDs in the inclinometer casing*: a full string is assembled by connecting a series of the FBG-SD sets. The end of a rigid segment is bolted to the end of a rigid segment from another set. The length of the rigid segments can be changed so that the distance between the neighbouring hinges can vary from 500 mm to as much as 2000 mm. The domains of FBG wavelengths are arranged so that four to five sets of the FBG-SDs share the same optical fibre. With the protective shielding, the outside diameter of the optical fibre is 3 mm, leaving sufficient room for the insertion of the FBG-SD and other optical fibres in an inclinometer casing.

(3) *FBG interrogation and interpretation of readings*: the optical fibres are connected to an FBG interrogator. The wavelength readings are converted to the degree of rotation at every hinge location according to the results of a single FBG-SD calibration obtained in step 1. Calculation of the lateral deflection of the full string of FBG-SDs is then made on the basis of the angle of rotation and length of each rigid segment.

The calibration of the FBG-SD, interpretation of the readings and effectiveness of the system are demonstrated in the following sections.

Laboratory calibration of a single FBG-SD unit

In the calibration of a single unit of the FBG-SD, one of the two rigid segments is fixed on a flat surface where rotation and sliding are not allowed. A mechanical caliper with a resolution of 1 μm is used to push or pull at a point of the second rigid segment laterally and thus causes a deflection angle, θ, or rotation of the second rigid segment against the hinge in degrees. The wavelength changes in the two FBGs, $\Delta\lambda_{B1}$ and $\Delta\lambda_{B2}$, are taken upon rotation of the segment. As indicated in equation (2), these FBG wavelength changes relate to the longitudinal strains within the two Bragg grating, ε_{B1} and ε_{B2}, respectively. Temperature effects and bending of the flexible segment can all contribute to ε_{B1} and ε_{B2}, so that

$$\varepsilon_{B1} = \varepsilon_T + \varepsilon_M \tag{4}$$

$$\varepsilon_{B2} = \varepsilon_T - \varepsilon_M \tag{5}$$

where ε_M is flexural strain, equal in magnitude but opposite in sign between the two FBGs, ε_T is longitudinal strain induced by thermal effects.

Subtracting equation (5) from (4) results in

$$\varepsilon_{B1} - \varepsilon_{B2} = 2\varepsilon_M \quad \text{or} \quad \varepsilon_M = \tfrac{1}{2}(\varepsilon_{B1} - \varepsilon_{B2}). \tag{6}$$

Figure 5 shows the relationship between $0.5(\Delta\lambda_{B1}-\Delta\lambda_{B2})$ and θ of an FBG-SD unit from a typical calibration test. The rigid segment was rotated from its neutral position by as much as 2.5° in both pull and push directions and the change of $0.5(\Delta\lambda_{B1}-\Delta\lambda_{B2})$ did not exceed 3000 pm. In the field applications, the segment rotations usually do not exceed 1°. Generally, the change in the wavelength within the FBG can reach 15 000 pm before losing linearity between $0.5(\Delta\lambda_{B1}-\Delta\lambda_{B2})$ and θ. For the case of figure 5, the FBG-SD has a calibration factor, the ratio of θ over $0.5(\Delta\lambda_{B1}-\Delta\lambda_{B2})$, of 0.0017° pm^{-1}. For an interrogation system with a 1 pm resolution, a deflection angle 0.0017° can be resolved using

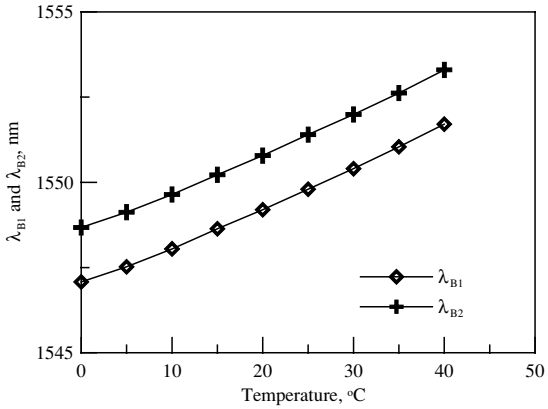

Figure 6. Calibration of the FBG readings in a temperature chamber.

the FBG-SD. Because of the importance of linearity between θ and $0.5(\Delta\lambda_{B1}-\Delta\lambda_{B2})$ readings in the interpretation of results, a quality assurance criterion was adopted. Upon calibration of the FBG-SD, a linear regression was carried out for the θ versus $0.5(\Delta\lambda_{B1}-\Delta\lambda_{B2})$ readings. The FBG-SD is rejected, if for any given θ within the data set, the corresponding $0.5(\Delta\lambda_{B1}-\Delta\lambda_{B2})$ reading (measured value) deviates more than 5 pm from the predicted value according to the linear regression (or |measured value − predicted value| > 5 pm). For the total of 30 FBG-SD units used in the indoor and outdoor experiments reported herein, the absolute value of the difference between the measured $0.5(\Delta\lambda_{B1}-\Delta\lambda_{B2})$ and that predicted by the linear regression for a given θ had an average of 2.62 pm and standard deviation (σ) of 3.11 pm.

A thermal calibration was performed by placing a unit of FBG-SD in a temperature chamber where the FBG-SD was subjected to a change of temperature from 0 to 40 °C. According to the results shown in figure 6, 1 degree of temperature change in Celsius (Δ °C) should correspond to approximately 115 pm in change of FBG wavelengths. These FBG wavelength changes are more significant than predicted by equation (3). The higher thermal sensitivity is likely due to the effects of epoxy and the plastic material to which the FBG was attached. To verify the effectiveness of the temperature compensation scheme, the FBG-SD was placed indoors where it was exposed to daily temperature fluctuations for a period of 1 week. The rigid segments were kept in their neutral position (no rotation) during the test. A time history of the wavelength change readings from the two FBGs, $\Delta\lambda_{B1}$ and $\Delta\lambda_{B2}$, as well as $0.5(\Delta\lambda_{B1}-\Delta\lambda_{B2})$ are plotted in figure 7. The record shows that the individual readings of $\Delta\lambda_{B1}$ and $\Delta\lambda_{B2}$ fluctuated by as much as 250 pm. The value of $0.5(\Delta\lambda_{B1}-\Delta\lambda_{B2})$ during the same period, however, did not exceed 1.7 pm, indicating that the scheme of subtracting one FBG reading from another was able to substantially offset the temperature effects.

Indoor verification of the FBG-SD system

To verify the effectiveness of the FBG-SD as a means to monitor ground movement, a series of experiments were conducted in the laboratory under controlled conditions. Two 9 m long inclinometer casings were tied together with steel blocks to assure that the two casings had the same amount

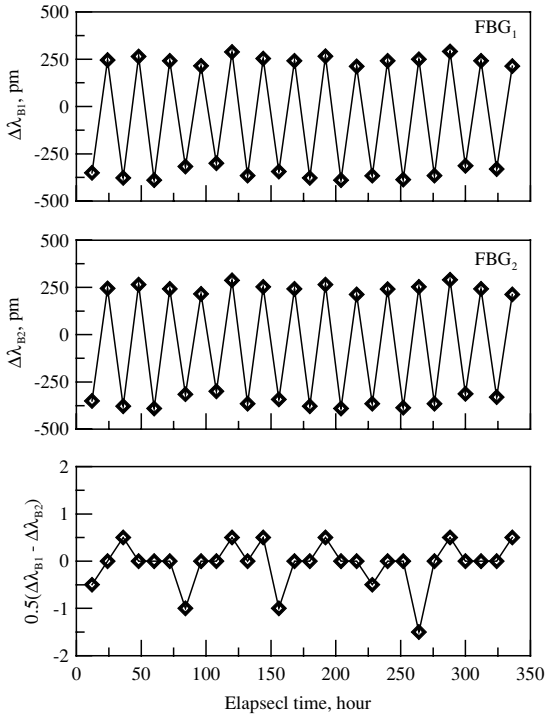

Figure 7. Effectiveness in offsetting temperature effects.

Table 1. Details of the FBG-SD units used in the indoor experiment.

Number	Depth of hinge (m)	Calibration factor (deg pm^{-1})
8	0.7	0.0020
7	1.7	0.0022
6	2.7	0.0018
5	3.7	0.0024
4	4.7	0.0024
3	5.7	0.0024
2	6.7	0.0020
1	7.7	0.0016

of lateral movement. The inclinometer casings were set up vertically against a stairway that was attached to a 3 m thick concrete reaction wall in a structural testing laboratory. A total of eight FBG-SD units were connected to form a string and inserted in one of the inclinometer casings. Table 1 shows the depth of the hinge locations and the calibration factor of all the FBG-SD units. The initial readings were taken for the FBG-SDs upon insertion. An IP was lowered into the other casing to establish the IP initial readings. The two inclinometer casings were then forced to deform simultaneously by pushing the steel blocks against the stairway. Upon fixing the casings in their deformed position, the FBG-SD and IP readings were taken again. Once inserted, the FBG-SDs were left in place throughout the experiment. Readings were taken by connecting the optic cables directly to the interrogator. For the IP, the probe was first lowered to the bottom and then raised in 500 mm intervals to take readings.

Figure 8 describes the development of the FBG-SD data from the original wavelength change readings to the lateral displacements. The vertical coordinate of the FBG-SD data symbols represents the depth location of the hinges in the FBG-SDs where the rotation between the neighbouring rigid

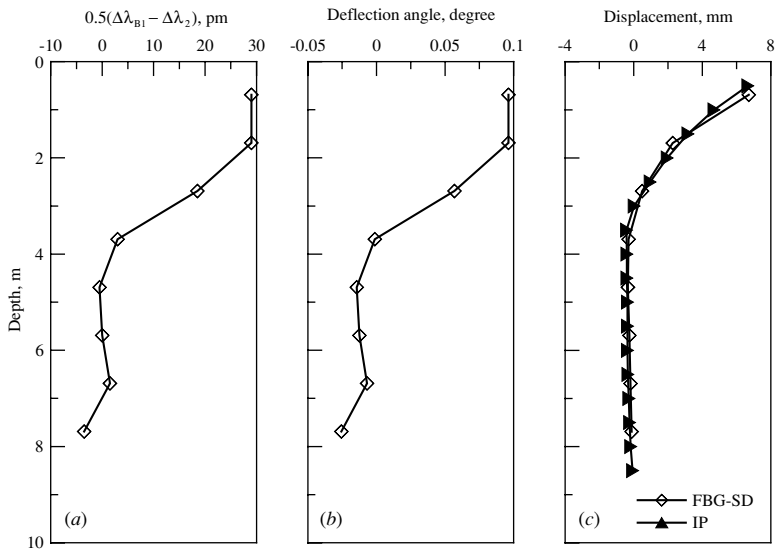

Figure 8. Development of lateral movement from wavelength changes.

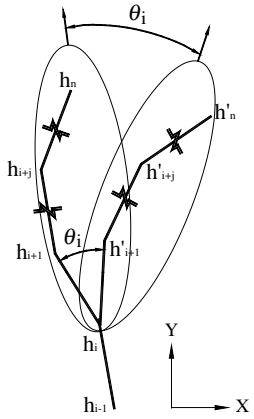

Figure 9. Computation of lateral movements as sequential rigid body rotations.

segments occurred. The wavelength change readings (current wavelength minus the original value prior to lateral movement) were first deducted and halved into $0.5(\Delta\lambda_{B1}-\Delta\lambda_{B2})$ as shown in figure 8(*a*) to offset the temperature effects. The deflection angle at each hinge location shown in figure 8(*b*) was then computed according to the values in figure 8(*a*) and the calibration results from the corresponding FBG-SD units as in the relationship shown in figure 5. To infer linear displacements from deflection angles, the FBG-SD units were treated as a series of rigid segments that were connected at hinges as shown in figure 8. Consider that there were n hinges in the series, denoted as $h_1, h_2, \ldots h_i \ldots h_n$, and h_1 was at the bottom. The rigid segment below h_1 was assumed to be fixed with no rotation. A stepwise procedure was used to compute the displacements due to the hinge deflections. If h_i deflected by an angle of θ_i from its original direction, then all the segments and hinges above h_i (i.e., from h_{i+1} to h_n) rotated

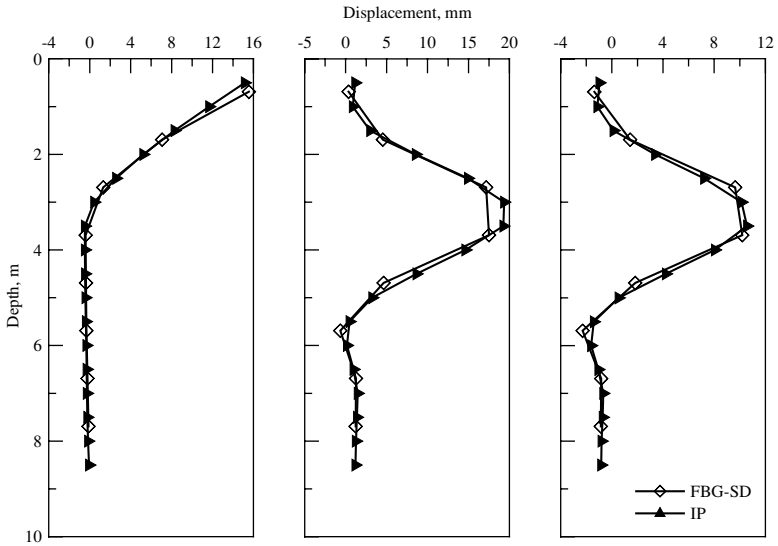

Figure 10. Comparison between FBG-SD and IP readings.

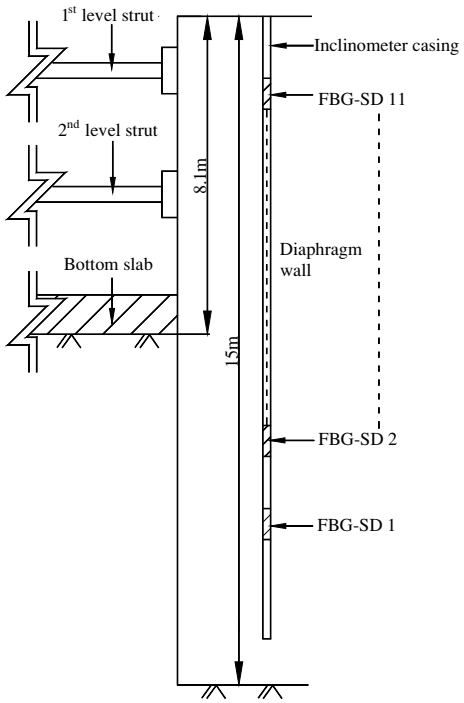

Figure 11. Schematic side view of the field set up.

as a rigid body by θ_i with respect to h_i as described in figure 9. The coordinates of all the hinges above h_i, or from h_{i+1} to h_n, were updated to those of h'_{i+1} to h'_n, on the basis of the rotated positions. This process of rigid body rotation and coordinate update was repeated from h_1 to h_n. The lateral movement at each hinge location in figure 8(c) was the difference in the x coordinate between the final updated position and its original position. A comparison between the results from FBG-SD and IP for various types and magnitudes of deformations are shown in figures 8(c) and 10. For all the indoor test data shown in figures 8(c) and 10, the absolute value of the difference in lateral movement measurements between FBG-SD and IP at comparable depths had an average of 1.32 mm and a σ of 2.38 mm. The maximum difference between the FBG-SD and IP measurements in these indoor experiments did not exceed 10% of the IP readings.

Field verification of the FBG-SD system

The FBG-SD system was tested in the field by monitoring the deformation of a 1.2 m thick, 15 m deep diaphragm wall during an internally braced deep excavation project in the Peitou district of Taipei. The foundation soil consisted of soft and sensitive silty clay. The 8.1 m deep excavation covered a square area of 100 m by 100 m, and was braced by two levels of cross lot struts. Two 14 m deep inclinometer casings spaced at 1 m were tied to the reinforcement cage and then fixed inside the diaphragm wall upon tremie concrete. Figure 11 shows a schematic side view of the field set up. The monitoring location was near the centre of one of the four excavation sides. A string of 11 FBG-SDs was inserted in one of the inclinometer casings leaving the other casing for IP measurements.

Figure 12 demonstrates the results from the FBG-SDs and IP readings at three stages of the excavation. Figure 12(a) shows the lateral movement induced by the pre-loading of the second level struts when the excavation reached 5.8 m. The pre-loading pushed the diaphragm wall outwards by as much as 2 mm. The monitoring results shown in figure 12(b) indicated that the diaphragm wall continued to move outwards by a maximum of 6 mm during a period of 14 days as the excavation extended to its final depth of 8.1 m. Upon reaching its final excavation depth, the placement of concrete formwork/reinforcement and the pouring of concrete for the bottom slab lasted 10 days. A comparison of the readings before and just after the completion of the bottom slab showed that the diaphragm wall moved inwards by as much as 11 mm as depicted in figure 12(c). The relatively large reversal

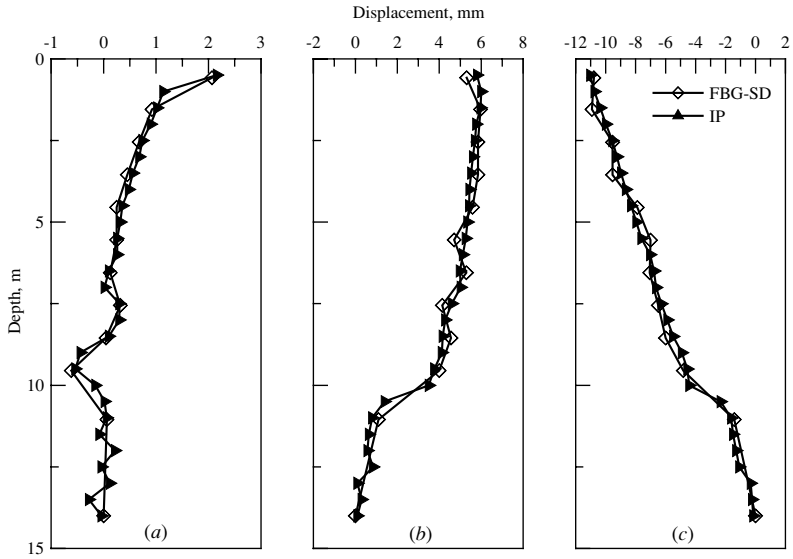

Figure 12. Comparison between FBG-SD and IP readings at three stages of excavation.

of the diaphragm wall movement was likely caused by heavy vehicles parked next to the diaphragm wall when the reinforcement steel and pre-mix concrete were delivered and a few days of heavy rainfall during the stage of the bottom slab construction. As in the case of indoor experiments, the ground movement according to the FBG-SDs was consistent with the IP readings. For all the field test data shown in figure 12, the absolute value of the difference in lateral movement measurements between the FBG-SD and the IP at comparable depths had an average of 1.03 mm and a σ of 1.79 mm.

Conclusions

The authors developed an FBG-based fibre optic sensor system mainly for the monitoring of ground movement. The laboratory and field experiments indicated that for the conditions applied, results comparable to those of a conventional IP can be obtained with the new FBG-SD sensor and the interrogation system. The FBG measurement was based on the peak value of the light wave which is relatively independent of the intensity variation of the light source. The FBG is a passive component which involves no circuitry placed underground. The material and method of signal transmission of the FBG are favourable for field geotechnical applications.

The computation of lateral movement is based on deflection angles measured at the FBG-SD hinge locations. The measurement error in the FBG-SD deflection angle at any given location is amplified with distance. This drawback may limit the length of the FBG-SD that can be used in the field. The FBG-SD monitoring system described in this paper has not been used for more than 4 months, which was the period of the excavation case described above. More applications are required to prove the longevity of the new system. It should be emphasized, however, that with the help of wheeled braces, replacement of the FBG-SD is rather simple as the units can be slid in and out of the inclinometer casing.

A series of patents related to the design concept of the FBG-SD have been filed.

References

Dunnicliff J 1988 *Geotechnical Instrumentation for Monitoring Field Performance* (New York: Wiley-Interscience) 253 pp

Dutro H B 1977 Borehole measurements using portable borehole deflectometers: *Proc. 18th Symp. on Rock Mechanics (Keystone, CO)* (Golden, Co: Colorado School of Mines Press) pp 5C4-1–5C4-5

Dyer S D, Williams P A, Espejo R J, Kofler J D and Etzel S M 2005 Fundamental limits in fiber Bragg grating peak wavelength measurements: *Proc. 17th Int. Conf. on Optical Fibre Sensors (Bruges, Belgium SPIE)* vol 5855 pp 88–93

Green G E and Mickkelsen P E 1988 Deformation measurements with inclinometers *Transportation Research Record 1169* (Washington, DC: TRB, National Research Council) pp 1–15

Hill K O, Fujii F, Johnson D C and Kawasaki B S 1978 Photosensitivity on optical fiber waveguides: application to reflection filter fabrication *Appl. Phys. Lett.* 32 647–9

Kersey A D 1992 Multiplexed fiber optic sensors *Proc. Fiber Optic Sensor (Boston, MA)* ed E Udd (SPIE—The International Society for Optical Engineering) pp 200–27

Kihara M, Hiramatsu K, Shima M and Ikeda S 2002 Distributed optical fiber strain sensor for detecting river embankment collapse *IEICE Trans. Electron.* **E-85-C** 952–60

Kumbhojkar A S, Israel T D, Arnstan D and Lee S M 1991 Development of a combination inclinometer–deflectometer and ADAAS *ASTM Geotech. Test. J.* **14** 451–6

Measures R M 2001 *Structural Monitoring with Fiber Optic Technology* (New York: Academic) 716 pp

Meltz G, Morey W W and Glam W H 1989 Formation of Bragg grating in optical fibers by transverse holographic method *Opt. Lett.* **14** 823–5

Mickkelsen P E 1996 Field instrumentation *Special Report 247 on Landslides Investigation and Mitigation* ed A K Turner and R L Schuster (Washington, DC: Transportation Research Board, National Research Council) pp 278–316

Naruse H, Uchiyama Y, Kurashima T and Unno S 2000 River levee change detection using distributed fiber optic strain sensor *IEICE Trans. Electron.* **E83-C** 462–7

Othonos A and Kalli K 1999 *Fiber Bragg Gratings: Fundamentals and Applications in Telecommunications and Sensing* (Boston, MA: Artech House) 422 pp

Rao Y J 1998 Fiber Bragg grating sensors: principles and applications *Optic Fiber Sensor Technology* vol 2, ed K T V Gattan and B T Meggitt (London: Chapman and Hall) pp 355–79

Yoshida Y, Kashiwai Y, Murakami E, Ishida S and Hashiguchi N 2002 Development of the monitoring System for slope deformations *Proc. SPIE* **4694** 296–302